Energy Reports 15 (2026) 108887

Contents lists available at ScienceDirect

Energy Reports

journal homepage: www.elsevier.com/locate/egyr

Research paper

Bi-level coordinated optimization method integrating improved artificial fish swarm algorithm and hardware cost model for distribution network

Zishun Peng [a,b], Yehong Li [a,*], Cao Li [a], Yuxing Dai [a], Kamal Al-Haddad [c], Wen Hu [a,*]

[a] National-local Joint Engineering Research Center for Digitalized Electrical Design Technology, Wenzhou University, Wenzhou, Zhejiang 325035, China
[b] Dongguan Digital Comprehensive Energy Engineering Technology Research Center, Dongguan, Guangdong 52300, China
[c] GREPCI, Ecole de Technologie Superieure, University of Quebec, Montreal H3C 2J2, Canada

ARTICLE INFO

Keywords:
Bi-level coordinated optimization Adaptive recombination
Fitness value
Hard device utilization cost
Improved artificial fish swarm algorithm
Power flow losses

ABSTRACT

Traditional power flow optimization fails to account for the coupling between network loss and the cost of converters, and overlooks both transmission loss and distribution equipment loss. This paper proposes a bi-level coordinated optimization framework that integrates an improved artificial fish swarm algorithm (AFSA) and a hardware cost model to resolve this conflict. This framework has developed a two-layer model consisting of an X-Y layer optimal power model and a Z-layer optimal reconstruction model, which explicitly combines hardware costs and inverter losses, effectively resolving the conflict between minimizing control actions and reducing system losses. Furthermore, an enhanced AFSA featuring adaptive recombination behavior significantly improves resource utilization efficiency and reduces computation time. The results verified on the experimental distribution network platform show that, compared with traditional methods, the proposed approach reduces the total economic cost by 7.97 %, enhances the wind power consumption capacity by 12.42 %, and increases the average minimum voltage by 6.81 %, while maintaining a comparable level of transmission loss.

1. Introduction

With the widespread penetration of distributed generation with inverters and power electronic devices in distribution network, the losses of equipment are gradually dominated by the losses of transformers and energy storage devices (Rahman et al., 2020; Zhao et al., 2022; Miao et al., 2018; Chen et al., 2023; Bayat et al., 2025). The losses in traditional distribution network mainly originate from transmission loss and losses in distribution equipment.The utilization frequency of transformers and energy storage has been enhanced to some extent through optimal power flow and distribution network reconfiguration, further increasing the proportion of losses in distribution equipment (Mahdavi et al., 2024a, 2024b; Song et al., 2022; Huang et al., 2023; Lejeune and Dehghanian, 2020; Fan et al., 2022).This implies that, in order to reduce losses in the distribution network and enhance its efficiency and economic feasibility, it is necessary to consider the coordinated optimization of distribution equipment and transmission losses (Gao et al., 2022; An et al., 2022; Liu et al., 2019; Zheng et al., 2021).

Previous studies have mainly focused on the optimization of transmission loss and the selection of distribution equipment locations and capacities. In (Chew et al., 2019; Yang et al., 2021; Li et al., 2025), the optimal power flow method was primarily employed to optimize the distribution network (Chew et al., 2019). proposed a binary integer load distribution model in order to optimize distribution losses and system voltage imbalance. A binary load allocation model was utilized to simplify the multi-objective problem and enhance voltage stability while reducing system losses (Yang et al., 2021). proposed an enhanced DistFlow model that replaced active and reactive power with their ratios to voltage magnitudes as state variables. This modification reduces the errors introduced by the traditional branch flow linearization method, which completely ignores the transmission loss term. As a result, the accuracy of power flow optimization is improved (Li et al., 2025). developed a two-level coordinated optimization model for transmission and distribution networks. By applying second-order cone relaxation to transform quadratic inequalities into standard conic form, the original problem was converted into a convex optimization problem that can be efficiently solved. This approach minimized load shedding and enhanced grid stability under extreme contingencies (Tavalaei et al., 2024; Al-Ismail, 2020; Huang et al., 2021). employed distribution network reconstruction to reduce network losses (Tavalaei et al., 2024). introduced an efficient mathematical optimization model integrating

* Correspondence to: Department of Electrical Engineering, Wenzhou University. Wenzhou. China.
E-mail addresses: pzswzu@wzu.edu.cn (Z. Peng), 23451247014@stu.wzu.edu.cn (Y. Li), 23451247007@stu.wzu.edu.cn (C. Li), daiyx@wzu.edu.cn (Y. Dai), kamal.al-haddad@etsmtl.ca (K. Al-Haddad), 20170194@wzu.edu.cn (W. Hu).

https://doi.org/10.1016/j.egyr.2025.12.024
Received 20 May 2025; Received in revised form 25 November 2025; Accepted 5 December 2025
Available online 13 December 2025

Nomenclature

Variable	Change in active power of node j
ΔP_j	Change in active power of node j
U_i	Voltage amplitude of node i
P_{j0}	Active input of node j at rated voltage
Q_{j0}	Reactive power input at node j under rated voltage
f_{set}	Set reference frequency
U_j	Node J voltage amplitude
G_{ji}	Conductivity between node j and node i
B_{ji}	The electronegativity between node j and node i
θ_{ji}	Voltage phase angle difference between node j and node i
ΔP_j^A	Changes in active power injected into port A
P_j^A	Active power injected into port A
g_i^A	Conductivity of Port A
θ_j	Voltage current phase angle difference at node j
b_i^H	Electromagnetic properties of H port
F_{loss}	system losses
P_{ij}^t	Active power of the line from node i to node j at time t
Q_{ij}^t	Reactive power of the line from node i to node j at time t
r_{ij}	Impedance of the line from node i to node j at time t
u_i^t	Voltage at node i at time t
$p_{sl,k}$	Switching Loss
$p_{ol,k}$	Conduction loss
g_{re}	Unit reconstruction loss cost coefficient
$P_{ess,k}^r$	Energy storage configuration power at node k
$E_{ess,k}^r$	Energy storage configuration capacity at node k
f_{inv}^{loss}	Transformer loss
f_{net}^{loss}	Network loss
f_{PQ}	Power quality
a_c,b_c	Converter switch loss coefficient
$i_{l,rms}$	Effective current value of the node l
$p_{wind,i,\Delta t}^{max}$	Peak output active power of the wind farm at node i during time period Δt
$p_{wind,i,\Delta t}$	The actual active power output of the wind farm at node i during the time period Δt
v_B^t	Node voltage at point B of the grid connection point
$U_{N,B}$	The Nth harmonic of the voltage at point B of the grid connection
v_l^t	Node voltage at port l at time t
v_l^{t-1}	Node voltage at port l at time t-1
F_{VS}	Voltage offset at the connection point of the power grid
F_{THD}	Voltage quality at the connection point of the power grid
F_{VF}	Voltage fluctuations at the connection points of the power grid
P_i	The total active power consumption of the inverter and the load connected to node i
Q_i	The total reactive power consumption of the inverter and the load connected to node i
$p_{b,t\pm\Delta t}^{max}$	Peak active power at point b near time t
$p_{b,t\pm\Delta t}^{min}$	The valley active power at point b near the point of grid connection at time t
$p_{ess,t\pm\Delta t}$	Corresponding energy storage operating power of $p_{b,t\pm\Delta t}^{max}$
$p_{ess,t\mp\Delta t}$	Corresponding energy storage operating power of $p_{b,t\pm\Delta t}^{min}$
X_i	The current position of the artificial fish
X_j	New location randomly selected by artificial fish
X_{next}	New position of artificial fish after movement
Y_c	Food concentration at the center position
Y_i	The food concentration at the current artificial fish location
Y_j	Food concentration at the optimal partner location
δ	Crowding concentration factor
n_f	Number of visible partners within the domain
K_i	Variation overlap index of artificial fish i
K_{imax}	The largest mutation overlap indicator in the current population
P	Recombination probability
$X_{k1,k2,k3}$	Three different individuals in the mutant fish population that meet the recombination criteria
X_{iDM}	Mutation candidate solution
Y_{iDM}	X_{iDM}'s food concentration
f_{fc}	food concentration
Parameters	Constant impedance load coefficient
α_i	Constant impedance load coefficient
β_i	Constant current load factor
γ_i	Constant power load factor
K_{Pa}	Frequency regulation coefficient
f	Frequency
T	Load frequency coefficient
N	Physical node
K	virtual node
K_{Qa}	Power regulation coefficient
F_{ji}	Equivalent connectivity matrix between node j and node i
H_{ji}	Equivalent interconnection matrix between node j and node i
Δt	time interval
s_{lc}	Life loss coefficient
s_{oc}	service factor
s_{mc}	maintenance factor
s_{p1}	Loss coefficient of node k switch
s_{p2}	Conductivity loss coefficient of node k
N_{re}	Accumulated usage times
N_{re}^{max}	Maximum available times
k_{de}	Equivalent annual depreciation coefficient for energy storage
k_{oc}	Energy storage operating cost coefficient
k_{mc}	Energy storage maintenance cost coefficient
$m_{inv,k}$	Transformer usage cost
$c_{ess,k}$	Energy storage usage cost
c_p	Unit power cost of energy storage
c_e	Unit capacity cost of energy storage
f_{hoc}	Hardware usage cost
$v_{ess,k}$	Energy storage utilization coefficient of node K
$v_{inv,g}$	Cost saving coefficient of node g inverter
Ω_{ess}	Inverter node set
Ω_{inv}	Collection of energy storage nodes
f_{wind}	Maximum wind power consumption capacity
$d_{1,2,3,4}$	Normalized weight factor
c_{wind}	Abandoned wind power price per unit of electricity
φ	Optimize time set
$v(i)$	A set of branch nodes with node i as the head end node
v_N	Rated voltage value
$i_{l,max}$	Upper limit of injected current at port l
$i_{l,min}$	Lower limit of injected current at port l
$v_{l,max}$	Upper limit of node voltage
$v_{l,min}$	Lower limit of node voltage
$p_{l,max}$	Upper limit of active power of node l
$p_{l,min}$	Lower limit of active power of node l
$Q_{l,max}$	The upper limit of reactive power of node l
$Q_{l,min}$	Lower limit of reactive power of node l
$p_{sl,k}^{max}$	Maximum switch loss at node k
$p_{sl,k}^{min}$	The minimum value of switch loss at node k
$p_{ol,k}^{max}$	The maximum value of conduction loss at node k
$p_{ol,k}^{min}$	Minimum value of conduction loss at node k

Step	Artificial fish movement step size	Visualperceived distance	coefficient of variation
R	A random number uniformly distributed within the interval [-1,1]	λ	coefficient of variation
		C_{iDM}	Cross probability threshold

network reconfiguration and disjunctive convex hull relaxation. By combining the strengths of generalized disjunctive programming and disjunctive convex hull relaxation, this approach optimizes distribution network reconfiguration, reducing computational burden while achieving minimized energy loss and enhanced grid stability.In (Al-Ismail, 2020), a novel voltage fluctuation index and optimization algorithm were proposed to regulate bus voltages by switching capacitor banks and optimizing network reconfiguration, reducing system transmission loss.In (Huang et al., 2021), leveraged deep learning to learn the relationship between network topology and short-term voltage stability from historical data, improving short-term voltage stability in conjunction with loss optimization. Previous studies incorporated considerations for energy storage locations and transformer capacities (Xiao et al., 2022; Macedo et al., 2015; Chennaif et al., 2022; Mahdavi et al., 2025). In (Xiao et al., 2022), the impact of energy storage integration was considered on a multi-objective model for network losses and voltage imbalance. The model was transformed into a convex quadratic programming problem, striking a balance between optimality and efficiency. In (Macedo et al., 2015), optimization of total loss in the distribution network was performed by controlling the reactive and active power, the number of switchable capacitor units, the tap positions of voltage regulators and on-load tap changers, and the operational status of energy storage devices (Chennaif et al., 2022). proposed an improved electric system cascade extended analysis (ESCEA) method, which takes into account the optimization objectives of power supply loss probability, life cycle cost, and levelized cost of energy, thus striking a balance between optimizing the new energy system and minimizing losses (Mahdavi et al., 2025). established a mixed integer convex optimization model accounting for time-varying load fluctuations. This approach enables simultaneous configuration of distributed generation (DG) units and capacitor banks, delivering enhanced accuracy in minimizing energy losses and operational costs. However, existing methods failed to simultaneously optimize both line losses and equipment losses. Furthermore, frequent control actions for energy storage and transformers during optimization often incurred high overall economic costs.

To reduce distribution equipment losses while optimizing transmission losses, it is necessary to incorporate operational constraints on each device into the optimization objectives (Zheng et al., 2016; Chen et al., 2022; Gao et al., 2019), In (Zheng et al., 2016; Chen et al., 2022), the operational constraints on compensation devices were introduced into the model, along with limitations on the utilization of various channels and distributed energy sources. This approach effectively restricted the maintenance costs associated with individual devices to some extent. In (Gao et al., 2019), the impact of changes in distribution system operating efficiency on transformer losses was considered in the optimization process, and a multi-objective approach was employed to minimize operating costs and total power losses using a genetic algorithm to obtain Pareto optimal solutions, resulting in a certain degree of cost reduction in the optimization process. While the above methods partially considered the losses of distribution equipment and imposed certain limitations, they did not account for the coupling relationship between distribution equipment losses and the optimization control actions. As the optimization process advanced, the magnitude of subsequent reduction in transmission losses becomes limited, while the adjustment frequency of devices such as transformers increased, exacerbating their losses. Therefore, an optimization method is required to address energy optimization comprehensively. It should also resolve the conflicting relationship between transmission loss optimization behavior and the hardware cost of distributed units.

Bi-level coordinated optimization method integrating improved artificial fish swarm algorithm and hardware cost model is proposed in this paper to address the previously mentioned issues. The method involves the incorporation of the optimization control behavior of transmission loss and hardware cost of distributed units into the bi-level optimization model. Moreover, the enhanced self-adaptation differential evolution based artificial fish swarm algorithm (SDAFSA) is proposed, which addresses the issue of the algorithm getting stuck in local optima by introducing self-adaptive recombination behavior during the fish swarm's mutation process.The main contributions of this paper are as follows:

- The proposed bi-level coordinated optimization method, which incorporates a converter loss model in the X-Y layer optimal power strategy and a hardware cost model in the Z layer optimal reconstruction strategy, can achieve the coordinated optimization between transmission losses and hardware utilization costs of distributed units. Therefore the economic efficiency of the system can be enhanced.
- The proposed improved artificial fish swarm algorithm, through the incorporation of an adaptive recombination behavior model in the variation process, enables an increase in the global optimization capability of the optimization parameters and a reduction in computation time and resource usage.
- Compared to the conventional artificial fish swarm algorithm based on differential evolution (DEAFSA), the designed self-adaptive recombination strategy in this study reduces the probability of repeated selection in the mutation process. This achievement allows for low memory usage and high optimization accuracy without affecting the computational time.

The remaining sections of this paper are organized as follows.

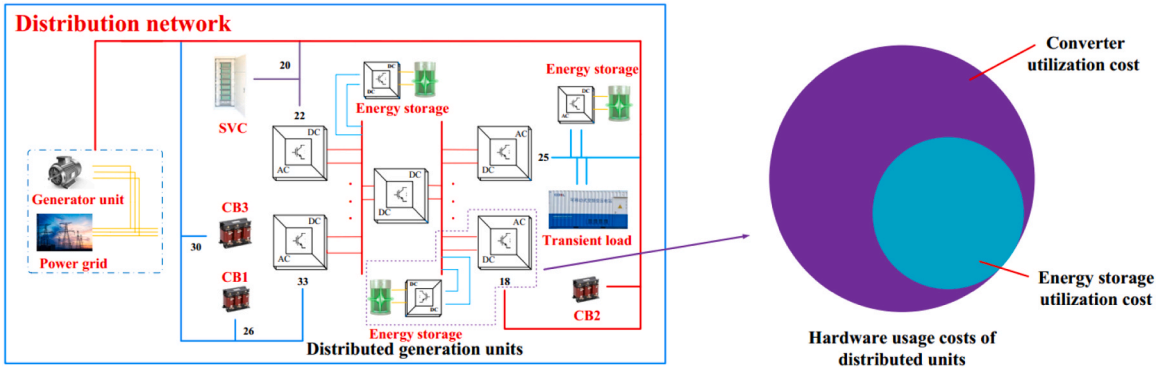

Fig. 1. Hardware cost analysis for distributed units in a distribution network.

Table 1
Analysis of the Impact of Key Nonlinear Parameter Fluctuations on System Cost Fluctuations.

S_{lc}(%)	s_{oc}(%)	s_{mc}(%)	k_{de}(%)	k_{oc}(%)	k_{mc}(%)	f_{hoc}(%)
0.99234438	0.98478440	0.93977834	0.86685580	0.84256282	0.97888142	0.96033910
0.83760700	0.94149655	0.85001048	0.92321067	0.83593701	0.95154889	0.97767119
0.89283558	0.96635571	0.86306491	0.97037001	0.90777741	0.85800149	0.99203857
0.9187035	0.88464562	0.96703928	0.92904706	0.83972180	0.98673472	0.96455701
0.9647549	0.9010810	0.9875736	0.8752930	0.8032160	0.92804701	0.95442321
0.88644344	0.96489699	0.80246830	0.90247281	0.86606449	0.90630873	0.99552230
0.96693395	0.93139751	0.85843779	0.92691412	0.95860111	0.86823248	0.99919729
0.90531141	0.84957093	0.84444330	0.84695962	0.90686940	0.85194974	0.97544664

Section 2 introduces the concept of distributed generation units, presents the model for evaluating the equipment utilization costs of distributed units, and analyzes the coupling relationship between the optimization behavior of transmission loss and the equipment utilization costs of distributed units. Based on this analysis, a bi-level coordinated optimization model is proposed. In Section 3, the SDAFSA algorithm is introduced, including the principle of self-adaptation recombination and the algorithm's optimization process. A comparative analysis of the computational cost of the algorithm is also provided. Section 4 presents experimental results and comparisons to validate the proposed approach. Lastly, Section 5 concludes the paper by summarizing the main findings.

2. The Bi-level coordinated optimization strategy

2.1. Analysis of modeling hardware costs for distributed units

The distributed generation units in the distribution network are shown in Fig. 1. In this unit, energy storage units are connected in parallel to the DC bus of the converter. For the purpose of modeling analysis and simplification,the virtual equivalent node method is introduced to equivalently represent the AC-DC nodes (Wu et al., 2021). The flow equation for network node injection is as follows:

$$\begin{aligned}&\Delta P_j = \left[\left(\alpha_i U_i^2 + \beta_i U_i + \gamma_i\right) P_{j0}\right]\cdot\left[1 + K_{Pa}(f - f_{set})T\right]\\&-U_j \sum_{i\in 1}^{N+K} U_i\left(G_{ji}\cos\theta_{ji} + B_{ji}\sin\theta_{ji}\right) = 0\end{aligned} \tag{1}$$

$$\begin{aligned}&\Delta Q_j = \left[\left(\alpha_i U_i^2 + \beta_i U_i + \gamma_i\right) Q_{j0}\right]\cdot\left[1 + K_{Qa}(f - f_{set})T\right]\\&-U_j \sum_{i\in 1}^{N+K} U_i\left(G_{ji}\cos\theta_{ji} + B_{ji}\sin\theta_{ji}\right) = 0\end{aligned} \tag{2}$$

The flow equation for port injection is as follows:

$$\begin{aligned}&\Delta P_j^A = P_j^A - g_i^A\left(\sum_{j=1}^{N+K} F_{ij}U_j\right)^2 + \sum_{j=1}^{N+K} F_{ij}U_j \sum_{j=1}^{N+K} H_{ij}U_j\cdot\\&\left\{g_i^A \cos\left[\sum_{j=1}^{N+K}\left(F_{ij} - H_{ij}\right)\theta_j\right]\right\} + \sum_{j=1}^{N+K} F_{ij}U_j\cdot\\&\sum_{j=1}^{N+K} H_{ij}U_j\left\{b_i^H \sin\left[\sum_{j=1}^{N+K}\left(F_{ij} - H_{ij}\right)\theta_j\right]\right\} = 0\end{aligned} \tag{3}$$

From Fig. 1, it can be observed that each distributed generation unit is a major component of the distribution network, and its usage cost accounts for a significant proportion of the overall system economic cost, considering both the transmission losses and the equipment costs.

Transmission losses mainly result from the energy losses in transmission and distribution lines (Azizi et al., 2023) and are expressed by (4). The usage cost of hard devices refers to the cost associated with the primary hardware components used in the distribution network, including the cost of energy storage and the cost of converters. The following introduces the modeling and analysis of energy storage usage costs and converter usage costs.

$$F_{loss} = \sum_{i=1}^{N}\sum_{j\in v(i)} \frac{\left(P_{ij}^t\right)^2 + \left(Q_{ij}^t\right)^2 \cdot r_{ij}\cdot\Delta t}{\left(u_i^t\right)^2} \tag{4}$$

The usage cost of converters $m_{inv,k}$ mainly includes the lifetime loss caused by reconstructions, routine operation, and maintenance of the equipment, as well as the switching and conduction losses under normal operating conditions. Considering that during the reconstruction process, the thermal stress generated by over current and over voltage due to structural changes is much greater than the switching losses under normal operating conditions, the lifetime loss coefficient is primarily determined by the number of reconstructions.This can be expressed by (5)-(6):

$$m_{inv,k} = s_{lc}(1 + s_{oc} + s_{mc})(s_{p1}p_{sl,k} + s_{p2}p_{ol,k}) \tag{5}$$

$$s_{lc} = g_{re}\cdot N_{re}/N_{re}^{\max} \tag{6}$$

where s_{lc}, s_{oc}, s_{mc}, s_{p1}, s_{p2}, $p_{sl,k}$, $p_{ol,k}$, g_{re}, N_{re}, N_{re}^{max} are the lifetime loss coefficient, operation coefficient, maintenance co-efficient, switching loss coefficient, conduction loss coefficient, switching, and conduction losses at node k,cumulative usage count, and maximum available count, respectively.

In practical applications, the over current voltage generated during reconstruction is often mitigated through energy storage to reduce transformer losses and lifetime degradation, leading to the introduction of the energy storage utilization cost function.

The energy storage utilization cost $c_{ess,k}$ primarily focuses on equipment operation costs and maintenance costs, which are converted into annual equivalent costs (Abomazid et al., 2022). Operation costs refer to the expenses incurred during the normal operation of the equipment, including energy consumption costs, maintenance costs, labor costs, etc. Maintenance costs, on the other hand, include regular maintenance costs and preventive maintenance costs required during normal operation. Considering that energy storage is used for over voltage and over current compensation in the transformer's DC bus during the reconstruction process, it can be expressed as shown in (7).

$$c_{ess,k} = k_{de}(1 + k_{oc} + k_{mc})(c_p p_{ess,k}^r + c_e E_{ess,k}^r) \tag{7}$$

where k_{de},k_{oc}, k_{mc},c_p, c_e,$P_{ess,k}^r$,and $E_{ess,k}^r$ are the annual equivalent depreciation coefficient of energy storage, the cost coefficient of an energy storage operation and maintenance, the cost per unit power and per unit capacity of energy storage, and the power and capacity of energy storage allocation at node k, respectively. Here, l= 1,2,……k.

The total equipment utilization costs of distributed units, denoted as f_{hoc}, is the sum of the usage costs of all energy storage and converter nodes. The energy storage utilization coefficient $v_{ess,k}$ is introduced to indicate the usage status of energy storage at a particular node, which takes a value of one when energy storage is connected and zero otherwise. When energy storage is connected, the usage cost of the converter decreases with the reduction of losses. Therefore, the cost-saving coefficient of the converter node, denoted as vinv,g, is expressed as follows:

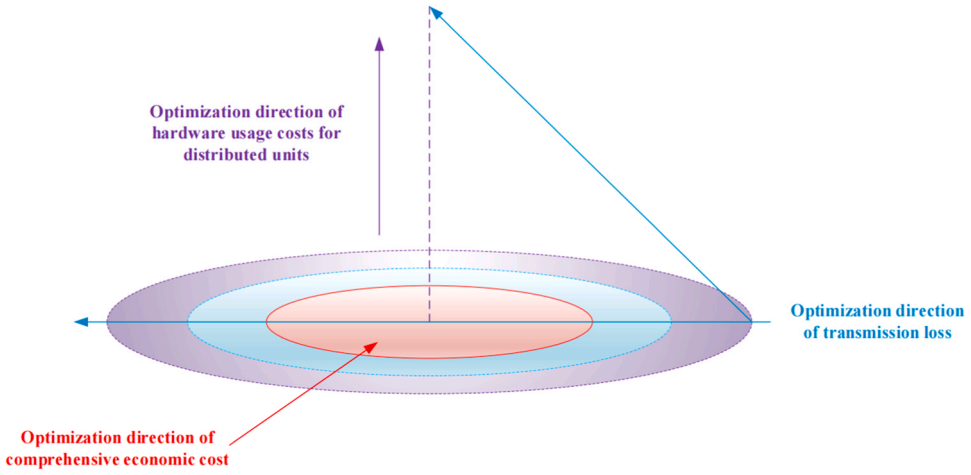

Fig. 2. Conflict between Transmission Loss and Hardware Cost.

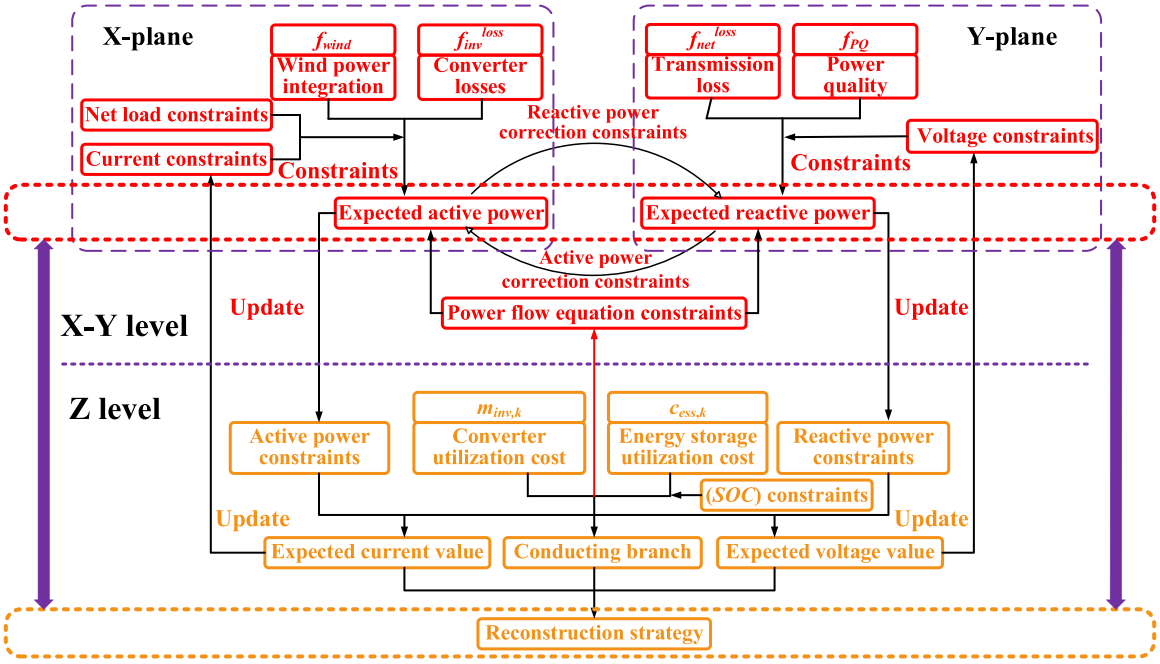

Fig. 3. Bi-level coordinated optimization model.

$$f_{hoc} = \sum_{\substack{k\in\Omega_{ess} \\ g\in\Omega_{inv}}} v_{ess,k}c_{ess,k} + v_{inv,g}m_{inv,g} \tag{8}$$

where $v_{ess,k}$, $v_{inv,g}$, Ω_{ess}, and Ω_{inv} are the energy storage utilization coefficient at node k, the cost-saving coefficient of the inverter node g, the set of inverter nodes, and the set of energy storage nodes, respectively. The value of $v_{inv,g}\in(0,1)$.

In order to evaluate the variability of cost correlation coefficients between converters and pure energy utilization, parameter robustness tests were conducted within the model. The f_{hoc} changes caused by ± 20 % random fluctuations in key nonlinear parameters such as Slc, Soc, Smc, Kde, Koc, and Kmc were tested. From the 10 sets of random test data in Table 1, it can be observed that the equipment utilization costs change by less than 5 %, indicating that the model still maintains strong stability and robustness under parameter uncertainty.

The conflicting relationship between equipment utilization costs of distributed units and transmission loss optimization behavior can be illustrated in Fig. 2, as derived from the comprehensive model. Without considering the optimization of hardware costs for distributed units, as transmission loss continues to be optimized, the system's economic cost improves. However, when transmission loss optimization exceeds the boundary, its projection no longer falls within the red region of optimal economic cost but enters the blue region of suboptimal economic cost. Nevertheless, through coordinated optimization of hardware costs for distributed units and transmission loss, the projection can be brought back within the optimal range of the system's economic cost.

2.2. The Bi-level optimization model

The bi-level coordinated optimization model is proposed in this section based on the coupling relationship between transmission loss optimization behavior and equipment utilization costs of distributed units, aiming to elucidate the coupling relationships among system variables and provide a foundation for control, as shown in Fig. 3. The model consists of the X-Y layers and the Z layer. In the Z layer, the reconstruction strategy is formed by combining basic reconstruction strategies according to the optimization objectives, and it changes with

the actual connection mode of the transformers.

2.2.1. X-Y layer optimization mode

Establish a comprehensive optimal power model at the X-Y layer, with wind power consumption f_{wind}, converter loss f_{inv}^{loss}, network loss f_{net}^{loss}, and power quality f_{PQ} as optimization objectives. Construct an optimization objective function through weighted linear combination as shown in Eq. 9, and constrain the sum of weight factors to 1 to achieve multi-objective normalization.

$$\min F = \min(d_1 f_{inv}^{loss} + d_2 f_{wind} + d_3 f_{net}^{loss} + d_4 f_{PQ}) \tag{9}$$

$$d_1 f_{inv}^{loss} + d_2 f_{wind} + d_3 f_{net}^{loss} + d_4 f_{PQ} = 1 \tag{10}$$

Among them, d1, d2, d3, and d4 are the corresponding weight factors for each function.

The loss equation of the converter is as follows:

$$f_{inv}^{loss} = \sum_{l=1}^{k} (a_c i_{l,rms}^2 + b_c i_{l,rms}) \tag{11}$$

Among them, a_c, b_c, $i_{l,rm}$ represent the switch loss coefficient and node effective current value, respectively.

The expression for the output of unconsolidated distributed power sources is as follows:

$$f_{wind} = \sum_{\Delta t \in \varphi} c_{wind} (P_{wind,i,\Delta t}^{max} - P_{wind,i,\Delta t}) \tag{12}$$

Among them, c_{wind}, $P_{wind,i,\triangle t}^{max}$, $P_{wind,i,\triangle t}$, respectively represent the abandoned wind power price per unit of electricity, the peak output active power and actual output active power of the wind farm at node i during the time periodΔt, and φ are the optimized time set.

The system network loss equation is as follows:

$$f_{net}^{loss} = \sum_{i=1}^{N} \sum_{j \in v(i)} \frac{(P_{ij}^t)^2 + (Q_{ij}^t)^2 \cdot r_{ij} \cdot \Delta t}{(u_i^t)^2} \tag{13}$$

Among them, P_{ij}^t, Q_{ij}^t, Representing the active and reactive power of the line from node i to node j at time t, r_{ij} represents the impedance of the line from node i to node j at time t, u_i^t is the voltage at node i at time t, and v(i) is the set of branch end nodes starting from node i.

The expressions for voltage offset F_{VS}, voltage quality F_{THD}, and voltage fluctuation F_{VF} at the grid connection point are as follows:

$$f_{PQ} = F_{VS} + F_{THD} + F_{VF} \tag{14}$$

$$F_{VS} = |(V_B{}^t - V_N)/V_N| \tag{15}$$

$$F_{THD} = \sqrt{\sum_{N=2}^{H} \left(\frac{U_{N,B}}{U_{1,B}}\right)} \tag{16}$$

$$F_{VF} = \sqrt{(V_l^t)^2 - (V_l^{t-1})^2} \tag{17}$$

Among them, V_B^t, V_N, $U_{N,B}$,V_l^t, V_l^{t-1} respectively represent the node voltage at grid point b and the rated voltage value, the Nth harmonic of the voltage at grid point b, and the node voltage at port l at time t and t-1. Among them, node i is the set of branch end nodes of the head end node.

The constraints of the X-Y layer include power flow equation constraints, net load constraints, current constraints, voltage constraints, active power constraints, and reactive power constraints.

The power flow equation can be expressed as:

$$\begin{cases} P_i = U_i \sum_{j \in i} U_j (G_{ij} \cos\theta_{ij} + B_{ij} \sin\theta_{ij}) \\ Q_i = U_i \sum_{j \in i} U_j (G_{ij} \sin\theta_{ij} - B_{ij} \cos\theta_{ij}) \end{cases}; i = 1, 2, \cdots, m \tag{18}$$

Among them, P_i、Q_i are the total active and reactive power values consumed by the converter and load connected to node i. U_i、U_j、G_{ij}、B_{ij}、θ_{ij} represent the voltage amplitude of nodes i and j, the conductance and susceptance between nodes i and j, and the phase angle difference between nodes i and j. j∈i represents all nodes connected to node i.

The constraints on the fluctuation range of net load at the grid connection point are as follows:

$$P_{flu}^{min} \le P_{flu} = \left|(P_{b,t\pm\Delta t}{}^{max} - P_{ess,t\pm\Delta t}) - (P_{b,t\pm\Delta t}{}^{min} - P_{ess,t\mp\Delta t})\right| \le P_{flu}^{max} \tag{19}$$

Among them,$P_{b,t\pm\Delta t}^{max}$、$P_{b,t\pm\Delta t}^{min}$ respectively represent the peak active power at node b near time t, and the valley power at node b near time t. $P_{ess,t\pm\Delta t}$、$P_{ess,t\mp\Delta t}$ are the energy storage operating power corresponding to the peak and valley active power at node b.

Current and voltage constraints are shown in Eqs. 20–21:

$$i_{l,\,max} < i_l < i_{l,\,min} \tag{20}$$

$$V_i^{min} < |V_i| < V_i^{max} \tag{21}$$

Among them, $i_{l,max}$, $i_{l,min}$, V_i^{max}, V_i^{min} are the upper and lower limits of the injected current at port l, and the upper and lower limits of the voltage at node i, respectively.

The constraints on active and reactive power of nodes are as shown in Eqs. 22–23:

$$P_{i,\,max} < P_i < P_{i,\,min}, i \in N \tag{22}$$

$$Q_{i,\,max} < Q_i < Q_{i,\,min}, i \in N \tag{23}$$

Among them, $P_{i,max}$, $P_{i,min}$, Q_i^{max}, Q_i^{min} are the upper and lower limits of voltage and reactive power at node i, respectively.

2.2.2. Z layer optimization model

The establishment of a comprehensive optimal reconstruction model for equipment utilization costs of distributed units fhoc in the Z layer. Its mathematical expression is as follows:

$$f_{hoc} = \sum_{\substack{k \in \Omega_{ess} \\ g \in \Omega_{inv}}} v_{ess,k} c_{ess,k} + v_{inv,g} m_{inv,g} \tag{24}$$

The constraints in the Z layer include power constraints on the converters and SOC(State of Charge) constraints. Its mathematical expression is as follows:

$$P_{sl,k}^{min} < P_{sl,k} < P_{sl,k}^{max} \tag{25}$$

$$P_{ol,k}^{min} < P_{ol,k} < P_{ol,k}^{max}, k \in N \tag{26}$$

where $p_{sl,k}^{min}$, $p_{sl,k}^{max}$, $p_{ol,k}^{min}$, and $p_{ol,k}^{max}$ are the maximum and minimum values of switch and conduction losses at node k, respectively.

The fundamental control principle of the proposed model is depicted in Fig. 3. When solving the X-layer model, the optimal active power expectation is determined to achieve the optimal wind power integration while minimizing converter losses, subject to constraints on netload fluctuations and currents at the grid connection point. The obtained active power expectation is then transferred to the Y-layer to update the reactive power constraints.In solving the Y-layer model, under voltage constraints,the expected reactive power that minimizes system transmission losses and maximizes power quality is computed. Simultaneously,the objective function value of the Y-layer, representing the expected reactive power, is fed back to the X-layer to adjust the constraints on active power generation. This process aims to refine the optimization results of the X-layer. Iterative steps are repeated to obtain the expected power values that minimize converter losses, minimize system transmission losses,and optimize wind power integration in the current network.Please note that the above translation is lengthy content and minor adjustments may be required to ensure accuracy and professionalism based on specific context and journal requirements. The

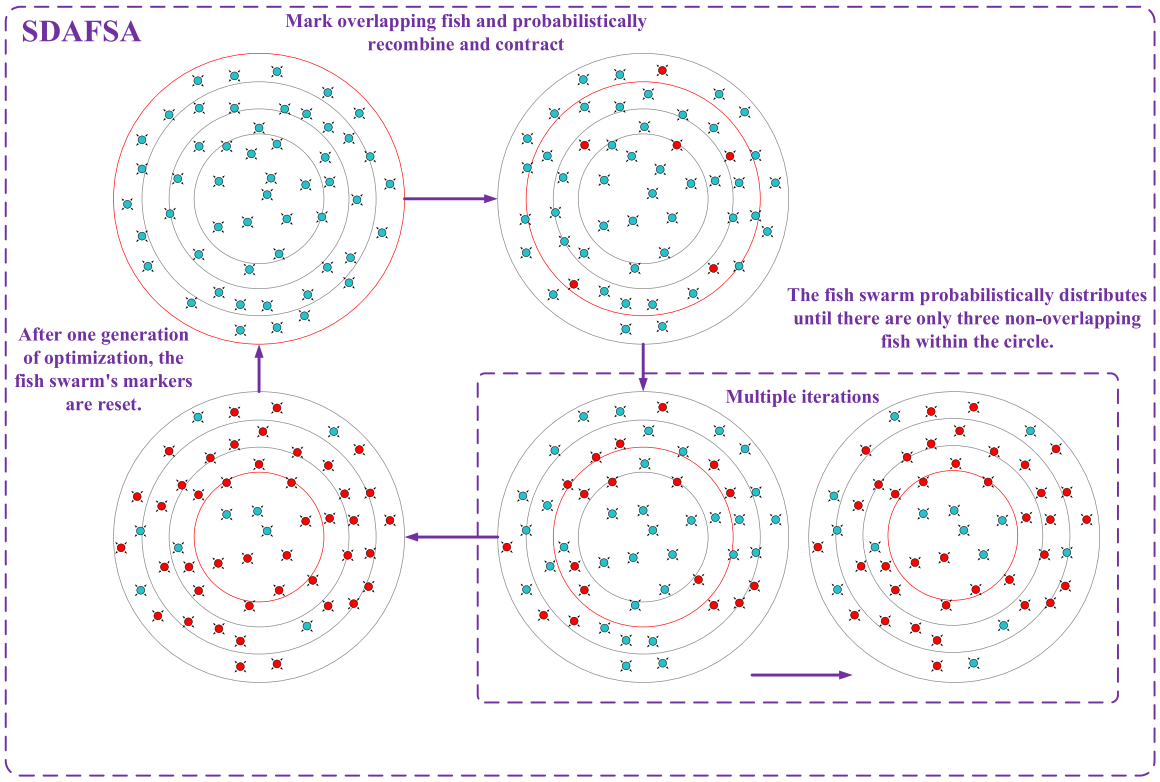

Fig. 4. Illustration of adaptive recombination.

X-Y layer's active and reactive power expectations are propagated to the Z lay- er. In the Z layer model,under constraints on active and reactive power, the expected currents,voltages,and conductive branches are computed to minimize converter and energy storage costs. Subsequently,the objective function values (Expected currents,Voltages,and Conductive branches) are returned to the X-Y layer current,voltage,and power flow equation constraints. By iteratively alternating between the top and bottom layers, the final reconstructed strategy is obtained,which achieves the minimum hard- ware usage costs of distributed units (including the converter and energy storage usage cost), the lowest system transmission loss, and the optimal wind power accommodation. Moreover, the expected power values under this reconstructed network are provided.

It can be observed from the previous context that the aforementioned constraints involve quadratic and integer terms. The solution of this model belongs to a nonlinear programming problem, which requires a considerable amount of computation time. The accuracy of traditional linear programming or nonlinear programming methods (Arnström et al., 2022; Sun and Sun, 2021) is difficult to guarantee,and they are not yet mature in handling inequality constraints.The DEAFSA has been gradually applied to distribution network optimization problems, exhibiting advantages such as low sensitivity to initial values and parameter (Sotiroudis et al., 2013; Bazi et al., 2014; Huang et al., 2015).

3. Adaptive recombination-based artificial fish swarm algorithm

In response to the issue of low optimization efficiency in the later stages of the algorithm caused by the blind mutation process of DEAFSA, this section proposes the SDAFSA to optimize the utilization of branch energy storage, the reconstruction of corresponding branches, as well as the voltage and current parameters of the transformers and energy storage nodes. The objective is to further enhance the coordination optimization performance of transmission losses and equipment utilization costs of distributed units. The specific details are presented as follows.

3.1. Traditional artificial fish swarm algorithm

The artificial fish swarm algorithm (AFSA), proposed by Li Xiaolei et al. in 2002, is a swarm intelligence optimization algorithm based on the behavior of autonomous animal communities. The control approach originated from the four fundamental behaviors observed in fish when they forage in water bodies. The traditional AFSA is commonly employed for single-layer optimization in distribution networks, such as reactive power optimization (Li et al., 2021; Zhu and Gao, 2020). It exhibits good performance and has advantages in terms of weak sensitivity to initial values and parameter selection, fast convergence speed, and robustness. However, in the later iterations of the AFSA, fish near the extremum point tend to repel each other, resulting in increased blind exploration of the fish swarm, slower speed, and lower optimization accuracy.

The mathematical description of the four behaviors of artificial fish is as follows:

(1) Foraging behavior

For the current state X_i of an artificial fish, a new state X_i is randomly selected within its perceptual range. If the food concentration at X_i exceeds that at the current position, the fish executes a movement operation toward X_i :

$$X_{inext} = X_i + rand() \cdot Step \cdot \frac{X_j - X_i}{\|X_j - X_i\|} \tag{27}$$

Otherwise, reselect X_i and re-evaluate the advancement condition. If no superior state is found within the maximum number of attempts, the fish moves randomly by one step:

$$X_{inext} = X_i + rand() \cdot Step \tag{28}$$

where rand denotes a random number uniformly distributed in the interval [0,1].

(2) Group behavior

Assuming the current state of the artificial fish is X_i, there are a

number of n_f partners in its visible domain ($d_{ij} \leq V_{isual}$), and the center positions X_j and concentrations Y_j of these partners can be obtained. In order to further optimize the exploration efficiency of fish schools, it is necessary to compare the concentration at the current location with the concentration at the center position Y_j of partners in the visible domain and the concentration at the current position under the crowding degree δ. This comparison process can be calculated using Eq. 29:

$$Y_c/n_f > \delta \cdot Y_i \tag{29}$$

If it is determined that the conditions are met, indicating that the partner's center position is rich in food and relatively less crowded, then the artificial fish will move forward one step towards that position; On the contrary, artificial fish perform foraging behavior.

(3) Rear end collision behavior

Assuming the current artificial fish is in the X_j state, the next decision is made by exploring the number of partners n_f and the partner X_j ($d_{ij} \leq V_{isual}$) with the highest food concentration in its visible domain. Compare the concentration Y_j near its partner's location with the current concentration Y_j under congestion δ., as shown in the equation:

$$Y_j/n_f > \delta \cdot Y_i \tag{30}$$

If the criteria are met, it indicates that there is more food available at partner Y_j's location and it is not too crowded, then move forward one step towards the partner's location; Otherwise, artificial fish will perform foraging behavior.

(4) Random behavior

Random behavior is actually a default behavior of foraging behavior, that is, the artificial fish randomly chooses a direction to move in the field of view, and the next position X_{inext} is represented as:

$$X_{inext} = X_i + r \cdot visual \tag{31}$$

Where r is a random number in the range of [-1,1], and visual is the perceived distance.

In the artificial fish swarm algorithm, the initialization of the artificial fish is first performed, followed by clustering and rear end behavior, exploring feasible positions and selecting the optimal position for movement within a certain number of times. During this process, a bulletin board was set up to record the optimal positions of all fish and their corresponding food concentrations after each position update. After completing the predetermined number of iterations, the algorithm stops.

3.2. The enhanced artificial fish swarm algorithm

In this paper, an improved algorithm called the SDAFSA is proposed based on the differential evolution (DE) algorithm. The SDAFSA introduces an adoptive recombination process, which effectively enhances mutation efficiency when encountering local optima.

After being trapped in local optima, the fish swarm undergoes adaptive recombination by utilizing a stagnation plate count to determine the entry into variation, as shown in Fig. 4. The fish from the previous iteration are marked as overlapping fish, and a probability, denoted as P, is set as the selection range for the variation fish. P is adaptively reduced as the number of overlapping fish increases. After each reduction, the fish positions are shuffled and updated, leading to a repetitive recombination process until the selection of mutated fish is completed. The selection of mutated fish includes mutation, crossover, and selection stages.

For each artificial fish, a mutation overlap indicator, K_i, and a recombination indicator, K_{imax}, are assigned. Additionally, a recombination probability P is defined. Random numbers denoted as rand are generated for all artificial fish, and each fish is associated with a corresponding random number,r_i. If r_i is less than P, three distinct individuals are selected from this subset for mutation using the differential evolution approach. After one iteration of differential evolution, the mutation overlap indicators are updated.

- Part 1-The adaptive recombination function

$$K_{i\,\max} = \{K_1, K_2 \ldots, K_i\} i \in (1, n_f) \tag{32}$$

$$P = 1 - K_{i\,\max}/n_f \tag{33}$$

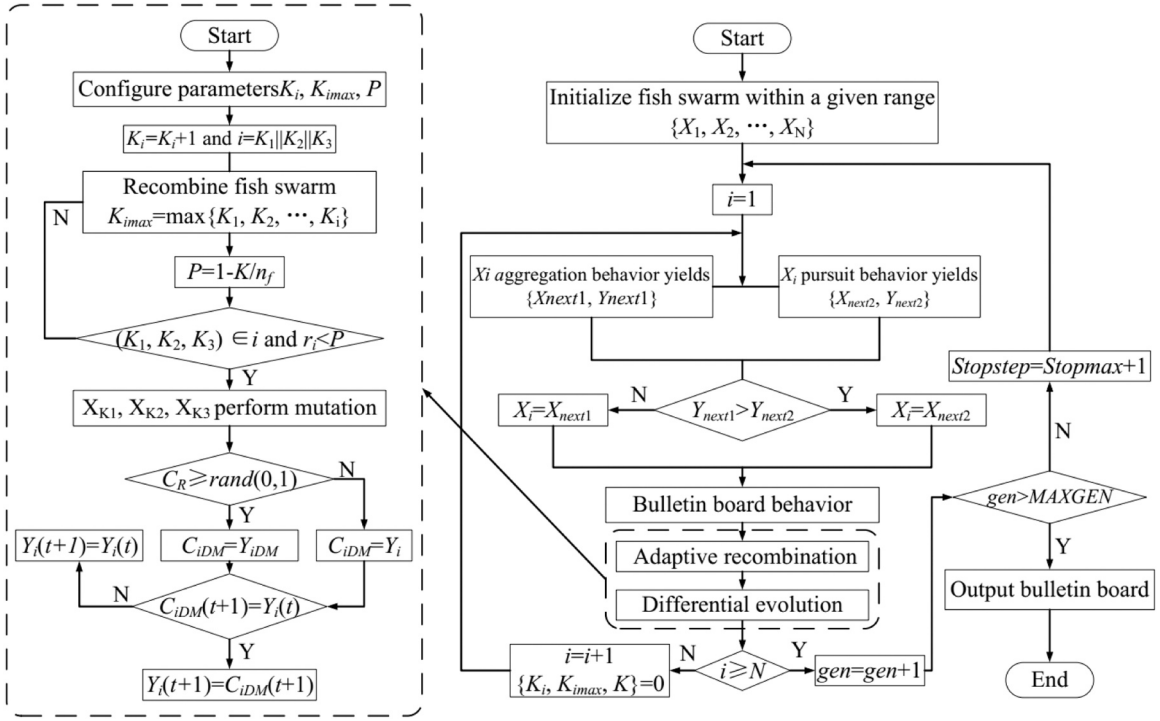

Fig. 5. The optimization process of the SDAFSA.

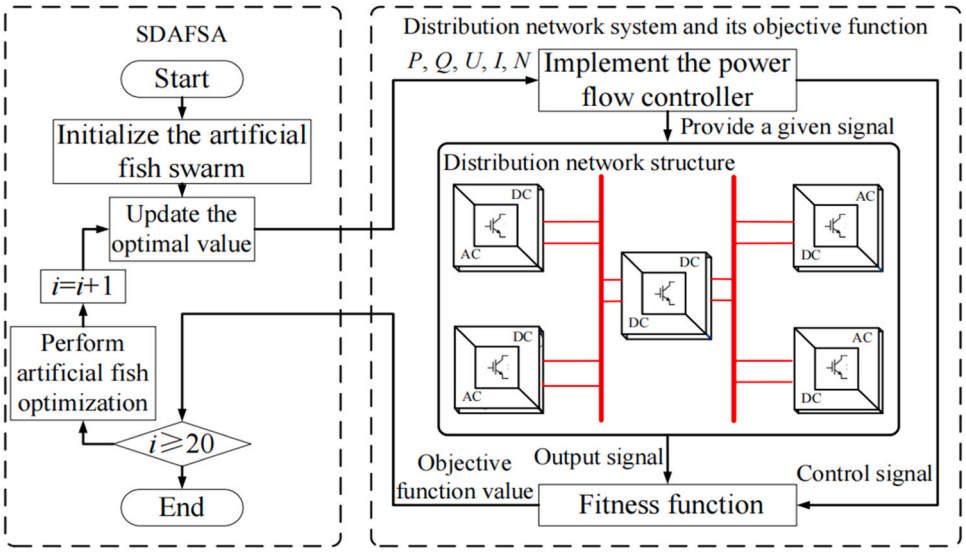

Fig. 6. Illustration of the optimization process of the SDAFSA.

- Part 2-Mutation

$$X_{iDM} = X_{k1} + \lambda \cdot rand() \cdot Step \cdot \frac{X_{k2} - X_{k3}}{\|X_{k2} - X_{k3}\|} \tag{34}$$

Three distinct individuals, k_1,k_2,and k_3, are selected from the artificial fish population that satisfies rand < P for mutation, according to the following (29), k_1,k_2,and k_3 represent the indices of randomly selected fish, and λ denotes the mutation coefficient.

- Part 3-Crossover

$$C_{iDM} = \begin{cases} Y_{iDM} & rand(0,1) \le C_R \\ Y_i & otherwise \end{cases} \tag{35}$$

Individual X_{iDM} is discretely crossed with the current population individual X_i according to (30),resulting in the differential individual fitness value C_{iDM}, where Y_i represents the current individual's food concentration, Y_{iDM} represents the target individual's food concentration after mutation, and CR denotes the crossover probability threshold.

- Part 4-Selection

The new individual $C_{iDM}(t+1)$ is compared with the corresponding fitness value of the current individual $X_i(t)$. If it is superior, the current individual is replaced.

3.3. Fitness function

The fitness function is the sole indicator for evaluating the optimization performance of the SDAFSA algorithm,with a higher fitness value indicating better optimization results.Since the coordination of transmission losses and hardware costs of distributed units aims to further reduce system economic costs, the bi-level coordinated optimization model can be defined as the fitness function, with the following expression:

$$f_{fc} = \frac{1}{F + f_{hoc}} \tag{36}$$

where f_{fc} is the food concentration function. As the coordinated optimization progresses,the food concentration function also increases. However,its actual value needs to be evaluated considering the practical application scenarios and hardware conditions.

The following is a detailed optimization process using the fitness function, as well as an explanation of its optimization in the distribution network.

3.4. Algorithm optimization process

The optimization process and schematic diagram of the SDAFSA algorithm are shown in Fig. 5 and Fig. 6,respectively.In Fig. 5,the recombination probability P is compared with the corresponding r_i value of each artificial fish,enabling the recombination of the fish population and the select- ion of mutated fish.The updated fitness value $Y_i(t+1)$ of the new individuals is achieved through the process of crossover selection.

The key steps of the SDAFSA for optimization are as follows:

- Step 1- The fish swarm is initialized.Throughout the entire process, the position X_{inext} and food concentration Y_i of artificial fish is updated based on the traditional artificial fish swarm position and food concentration function.
- Step 2- The artificial fish are encoded. The initial fitness value of the fish swarm is calculated,and the fittest individual is searched for and recorded on the bulletin board.The bulletin board is set to a stagnant state with Stopstep= 0, and the iteration count is gen= 1.
- Step 3- Behavior selection.Simulate four types of behaviors: clustering, following, foraging, and random behavior. After each iteration of an individual artificial fish, its own state is compared with the records on the bulletin board.If it is superior to the bulletin board records,the bulletin board is updated and the bulletin board's stagnation step is set to Stopstep= 0.
- Step 4- Stagnation evaluation. Evaluate if Stopstep≥Stopmax (maximum stagnation steps). If this condition is satisfied, perform adaptive recombination and differential evolution on the entire population of artificial fish. Otherwise, proceed to Step 5.
- Step 5- Iteration limit evaluation. Evaluate if gen>MAXGEN, indicating the maximum number of iterations has been reached. If this condition is satisfied, output the optimal solution. If not, update the stagnation step of the bulletin board and proceed to Step 3.

The key steps of adaptive recombination are as follows:

Table 2
Computational time cost.

	AFSA	SDAFSA	DEAFSA
Algorithm execution time			
t_s	×	7.49352 s	×
t_d	×	3.50592 s	7.71336 s
t_a	147.7932 s	156.38263 s	154.61752 s

Table 3
Resource utilization cost (memory usage).

	AFSA	SDAFSA	DEAFSA
Algorithm execution time			
Algorithm execution time	×	×	6 K
Differential Evolution	×	40 K	24 K
Differential Evolution	25120 K	25144 K	25138 K

- Step 1- Configuration Parameters: The configuration parameters include the mutation overlap indicator K_i, recombination indicator K_{imax}, recombination probability P, and random number r_i corresponding to the artificial fish. The values of K_{imax} and P are updated using (27)-(28) respectively. The mutation position X_{iDM} and mutation fitness value Y_{iDM} are updated using (29)-(30) respectively.
- Step 2- Adaptive Recombination: The process involves evaluating the indices of the mutated fish and the indices of the previously mutated fish to determine the overlap indicator, K_i. The extreme value is recorded as K_{imax} and an artificial fish with a random number r_i less than the recombination probability P is selected as the mutated fish.
- Step 3- Mutation Operation: Select artificial fish that meet the given criteria and subject them to the mutation process to obtain individual X_{iDM}.
- Step 4- Crossover Operation: The individual X_{iDM} is subjected to discrete crossover with the current individual Xi in the population. By comparing the cross-over rate C_R with a random number rand (0,1),the fitness value C_{iDM} of the differential individual is updated.
- Step 5- Selection Operation: The new individual $C_{iDM}(t+1)$ is compared with the fitness value of the current individual $X_i(t)$. If it is superior, the current individual is replaced.

As shown in Fig. 6, the input signals of the fitness function are composed of the output signals from each converter, as well as the load output signals and the power flow control signals of the system. The fitness value is obtained through the fitness function. The improved Artificial Fish Swarm Algorithm searches for the optimal parameters P, Q, V, I,and N by evaluating the fitness function value at each iteration until the end of the iteration.

3.5. Cost comparison calculation

Compared to DEAFSA, SDAFSA incorporates an additional step of adaptive recombination, which requires consideration of the computational cost associated with this step. The cost calculation mainly includes resource utilization and computational time,with the total computational time denoted as t_a.

Adaptive Recombination: The computational time t_s can be divided into two components: the time for adaptive narrowing of the fish selection range,t_{s1}, and the time for random updating of fish positions, t_{s2}. Differential Evolution: The computational time t_d can be divided into three components: the time for mutation td1, the time for crossover t_{d2}, and the time for selection t_{d3}.

For the simulation hardware,a 64-bit PC with a Windows 7 operating system is utilized. The CPU is an i5–11300H with a clock frequency of 3.0 GHz. The system has 16 GB of RAM and a hard disk capacity of 500 GB.

As shown in Tables 2 and 3,in the SDAFSA algorithm,the computational time for the mutation step after adaptive recombination, denoted as t_d, is reduced by approximately 54.55 % compared to the computational time for the mutation step in the DEAFSA,denoted as t_d. Additionally, resource utilization is reduced by 40 %. The combined resource utilization of adaptive recombination and differential evolution is reduced by 25 %. This indicates that adaptive recombination improves the effectiveness of repetitive mutation.

The total computation time ta of SDAFSA differs by 5.812 % and 1.142 %compared to AFSA and DEAFSA, respectively. The difference in total resources is below 1 % for both cases and slightly lower than the total resource usage of DEAFSA. It can be observed that the inclusion of adaptive recombination has no significant impact on the computational speed and provides some optimization in terms of resource utilization compared to DEAFSA.

Table 4
Grid connection parameters.

Node	Type	Parameters	Quantity
8	Wind power	150KW	1
26	CB1	150KVA	5
18	CB2	150KVA	5
30	CB3	150KVA	5
20	SVC	0–500KVA	1
25	Energy storage	1 MW	1
25	Impulsive load	0–800KW	1

Table 5
Basic reactive power compensation strategies.

Node	Type	Parameters
26	CB1	0–5
18	CB2	0–5
30	CB3	0–5
20	SVC	0–500KVA

4. Experimental comparative verification

To validate the superior optimization performance of SDAFSA and the bi-level coordinated optimization method compared to the traditional method under load impact, a simulation model was established for conducting experimental analysis. The simulation model consists of two parts: the distribution network structure and the transformer structure.

The application scenario for the distribution network is set as a port distribution network, and the distribution network model selected is the IEEE 33-node model. The IEEE 33 node system is a recognized benchmark testing system in distribution network research, and its topology and load characteristics are representative, which can fully verify the effectiveness and generalization ability of the method proposed in this paper. The load section is set as the port load, and actual parameters of port impact load, distributed energy sources, SVC, energy storage, etc., are incorporated into the model. The transformer connection is implemented using an energy router structure (Liu et al., 2021; Wang et al., 2022), connecting nodes 22, 33, 18,and 25, which provides flexibility and enables basic reconstruction strategies.The input parameters are obtained from the partial model parameters of the IEEE 33-node system and the operational parameters of the actual port shore power project over a 24-hour period. The input parameters are shown in Table 4, and the basic strategies for reactive power compensation are shown in Table 5. CB1, CB2, and CB3 represent reactive power compensators.

4.1. Performance experiment comparison

The parameter settings of SDAFSA algorithm are as follows: visual= 1, step= 0.1, λ= 0.86. By comparing the computation time spent iterating to the optimal solution under different parameters in Table 6,

Table 6
SDAFSA computation time under different parameters.

group	1	2	3	4	5	6	7	8	9	10
visual	0.4	0.67	0.78	0.88	0.94	0.98	1	1.1	1.2	1.5
step	0.8	0.56	0.32	0.18	0.14	0.12	0.1	0.08	0.06	0.03
λ	2	1.6	1.2	1	0.95	0.9	0.86	0.84	0.82	0.74
Time(s)	249.9021	233.8633	213.1426	192.2057	179.5354	170.6098	167.3821	181.7582	224.0994	257.4234

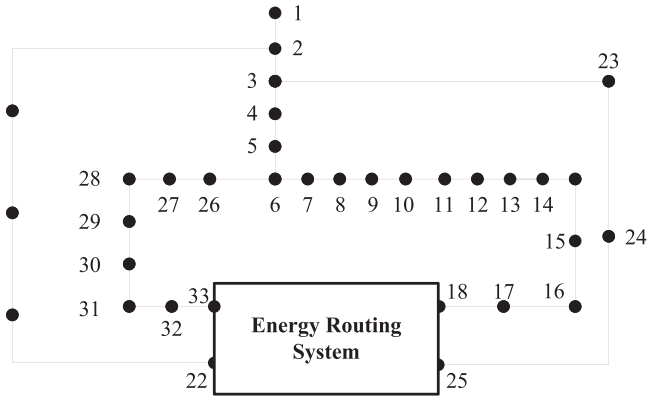

Fig. 7. 33-node distribution network diagram.

this parameter is determined to be the optimal parameter. The artificial fish numbers for the three fish swarm algorithms are all 12, while the particle swarm algorithm (PSO) has 12 particles, inertia weight w= 0.7, cognitive factor c1 = 1.5, social factor c2 = 1.5. The genetic algorithm (GA) has a population size of 12, crossover probability Pc= 0.8, mutation probability Pm= 0.02, and elite retention ratio of 0.1.The grey wolf optimization (GWO) algorithm involves 12 wolves. The convergence factor a decreases linearly from 2 to 0 as the number of iterations increases, and the moduli of the coefficient vectors r1 and r2 are randomly selected from the interval [0,1] (Mirjalili et al., 2014). The maximum number of iterations is set to 20, and the number of attempts is set to 10. The performance of six algorithms was compared, and the corresponding convergence characteristic curves are shown in Figs. 7 and 8. The fitness and other indicators are shown in Table 7. The parameters of the energy storage part of the algorithm are shown in Table 6.

Compared with traditional AFSA, PSO, GA, and GWO algorithms, PSO has the fastest convergence speed but a lower fitness value, while GA algorithm has the highest fitness value but a slower convergence speed, while AFSA balances both convergence speed and fitness value.

The following table shows the maximum, minimum, and average fitness values of the objective function for twenty independent runs of AFSA, DEAFSA, PSO, GA, GWO, and SDAFSA algorithms. The maximum, minimum, mean, and standard deviation of SDAFSA are all greater than those of traditional AFSA, PSO, GA, GWO, and DEAFSA algorithms. Therefore, the SDAFSA algorithm is superior to traditional AFSA, PSO, GA, GWO, and DEAFSA algorithms. Compared to traditional AFSA, PSO, GA, GWO, and DEAFSA, it exhibits outstanding global search capabilities.

According to Fig. 8, DEASFA and AFSA fell into local optima in the 5th and 14th iterations, PSO, GA, and GWO fell into local optima in the

Table 7
Algorithm optimization comparison.

Algorithm	Maximum Fitness	Average Fitness	Average Fitness
SDAFSA	1.58161	1.55181	1.52139
AFSA	1.47324	1.45175	1.39704
DEAFSA	1.53419	1.51286	1.48315
PSO	1.45832	1.41323	1.36672
GA	1.48661	1.46892	1.44774
GWO	1.46326	1.43717	1.38331

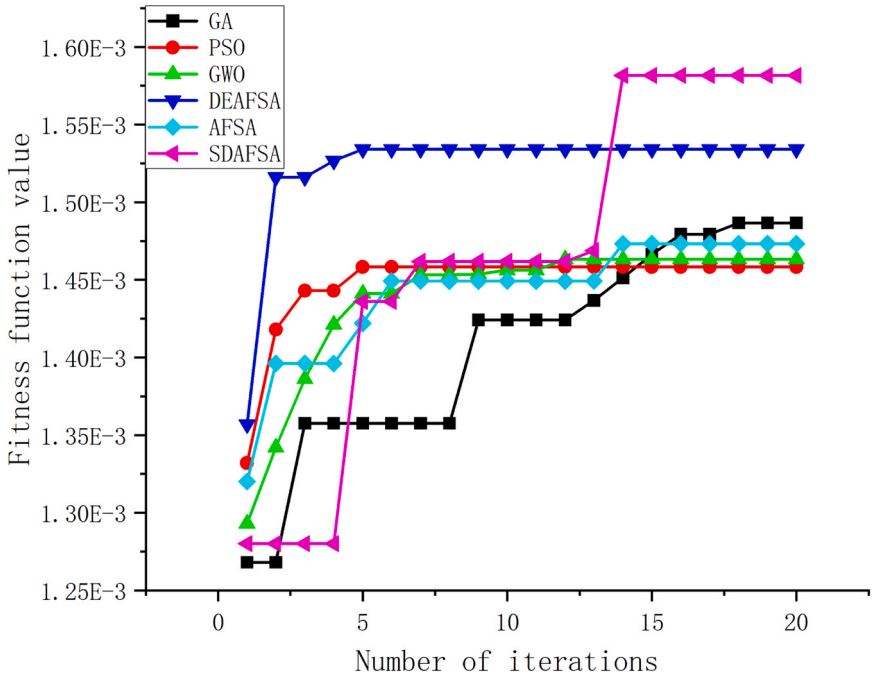

Fig. 8. Algorithm convergence characteristics comparison chart.

Table 8
Modes.

Conditions	Conditions	Maximum rate of change of shore power	Number of accesses
1	800KW	0.975	1
2	200KW	0.51	4

Table 9
Grid connection parameters.

	Power loss (MW)	Voltage mean (per unit value)	Converter utilization cost (in million RMB)	Energy storage utilization cost (in million RMB)
mode 1				
Conventional methods	0.131	0.88	542.11	66.23
Bi-level coordinated optimization (DEAFSA)	0.140	0.93	519.53	58.74
Bi-level coordinated optimization (SDAFSA)	0.134	0.94	507.04	52.73
mode 2				
Conventional methods	0.123	0.89	531.05	64.41
Bi-level coordinated optimization (DEAFSA)	0.132	0.95	498.53	56.89
Bi-level coordinated optimization (SDAFSA)	0.125	0.97	486.42	49.06

5th, 18th, and 12th iterations, respectively. SDAFSA (an improved artificial fish swarm algorithm based on adaptive recombination) found the optimal fitness value in the 14th iteration after falling into local optima in the 7th iteration. As evidenced by Table 7 across 20 independent trials, the optimal fitness values demonstrate the hierarchy: SDAFSA > DEAFSA > GA > AFSA > GWO > PSO. The proposed improvements yield a 6.89 % increase in optimal fitness performance.

4.2. Experimental comparison of optimization methods

A comparative experiment evaluates the proposed bi-level coordinated optimization method against a traditional optimal power flow method (minimizing transmission loss) under two distinct shore power load variation scenarios. Both scenarios share the same total connected shore power capacity but differ in the rate of change and capacities of individual units. The experiment aims to validate the superior optimization performance of the proposed method under both high-impact and lower-impact load conditions. The proposed method employs both SDAFSA and DEAFSA algorithms, with results averaged over twenty iterations. Key metrics include branch currents, voltage fluctuations, dynamic transmission losses, the equipment utilization costs of distributed units, and overall economic loss. The modes are presented in Table 8 and the specific optimization indicators before and after improvement for the bi-level coordinated optimization method are provided in Table 9.

Under the proposed coordinated optimization, the port's integrated power supply system dynamically executes combinations of six basic reconfiguration strategies across 24 time intervals (Fig. 11 and Fig. 12). Energy storage operates within an SOC range of (0.1, 0.9), with charge strategies depicted in Fig. 13 and Fig. 14. The most frequently utilized grid operating diagrams from the reconfiguration strategies are presented in Fig. 9 and Fig. 10. Dynamic transmission losses, voltage fluctuations, branch power flows, and wind power integration are compared against the traditional method in Figs. 11–15.

Mode 1:With the variation of shore power load, the maximum rate of change within a 2–3 h period reaches 0.975.From Table 8 and Fig. 15(a) and Fig. 16(a), it can be observed that compared to the traditional method, the bi-level coordinated optimization method using the DEAFSA and SDAFSA algorithms increases the total transmission losses by approximately 6.81 % and 2.29 % respectively.

The average minimum voltage at each time interval is increased by approximately 5.68 % and 6.81 % respectively. The branch power flow losses are increased by approximately 4.09 % and 1.63 % respectively. The wind power integration is improved by approximately 8.61 % and 12.42 % respectively.Under high-impact loads, the system's economic performance is significantly improved with a minor impact on transmission losses. The overall economic losses are reduced by approximately 4.93 % and 7.97 % respectively.

Mode 2: With the variation of shore power load, the maximum rate of change reaches 0.51 during hours 8–9.According to Table 8, Mode 2,

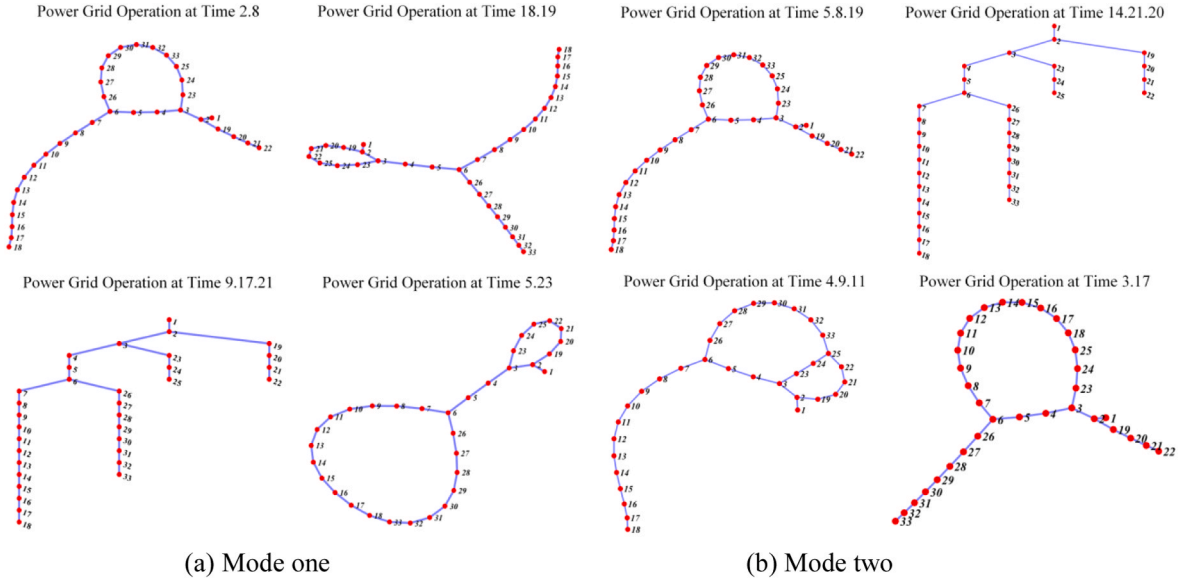

Fig. 9. Typical operating node diagram under bi-level coordinated optimization(DEAFSA).

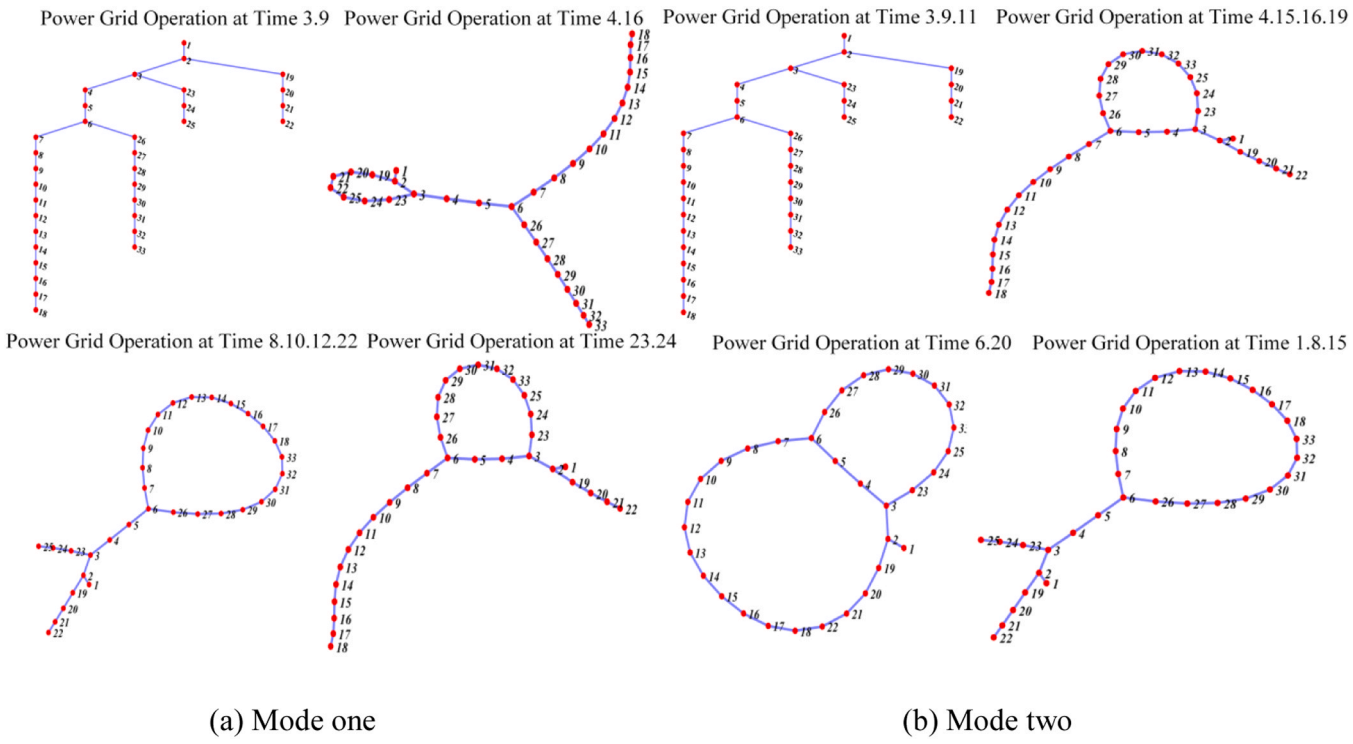

Fig. 10. Typical operating node diagram under Bi-level coordinated optimization(SDAFSA).

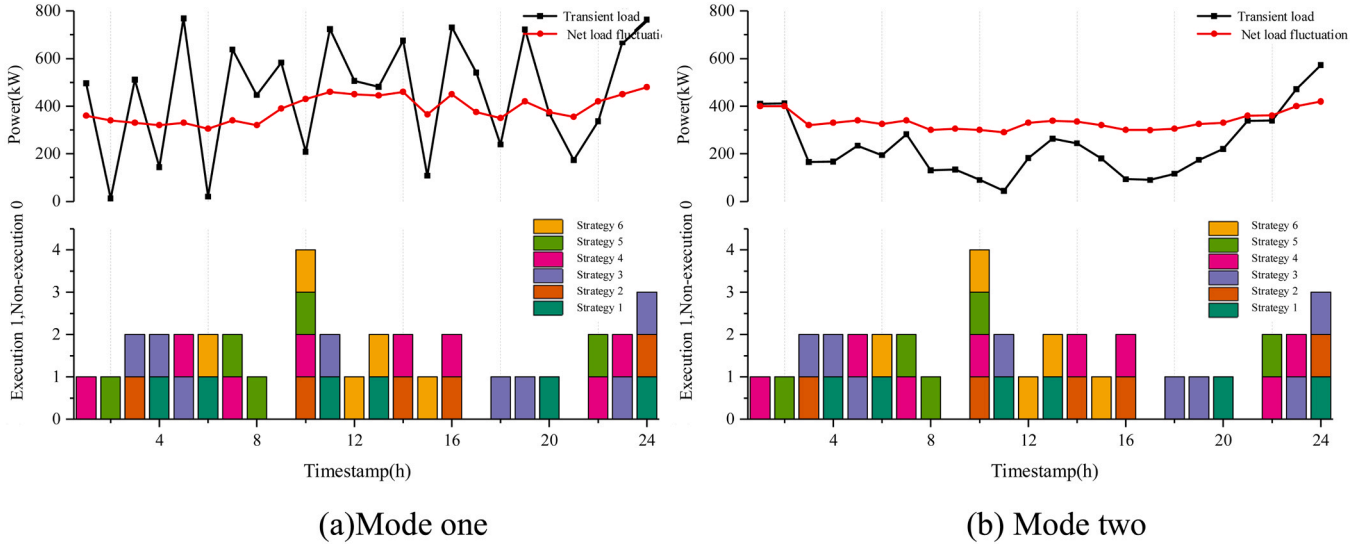

Fig. 11. Transient load and routing strategy (DEAFSA).

and Fig. 15(b) and Fig. 16(b), it can be observed that compared to the traditional method, the bi-level coordinated optimization method using the DEAFSA and SDAFSA algorithms increases the total transmission losses by approximately 7.31 % and 1.63 %, respectively.

The average voltage at each time interval is increased by approximately 6.74 % and 8.98 %, respectively. The branch power flow losses are increased by approximately 6.09 % and 2.81 %, respectively.The wind power integration is improved by approximately 2.95 % and 2.80 %, respectively. The overall economic losses are reduced by approximately 6.71 % and 9.98 %, respectively.

These findings demonstrate that the method exhibits favorable economic performance and control effectiveness under high-impact loads. In conclusion, the proposed bi-level coordinated optimization method outperforms the traditional optimization method under both Modes. Additionally, when comparing the SDAFSA algorithm to the DEAFSA algorithm, it shows good optimization effects for dynamic transmission losses, voltage fluctuations, branch power flows, wind power integration,and overall economic costs.

5. Conclusion

A dual layer coordinated optimization method integrating improved artificial fish swarm algorithm and hardware cost model is proposed. The proposed dual layer coordinated optimization method incorporates the converter loss model and hardware cost model into the dual layer optimization framework, and adopts an improved artificial fish swarm

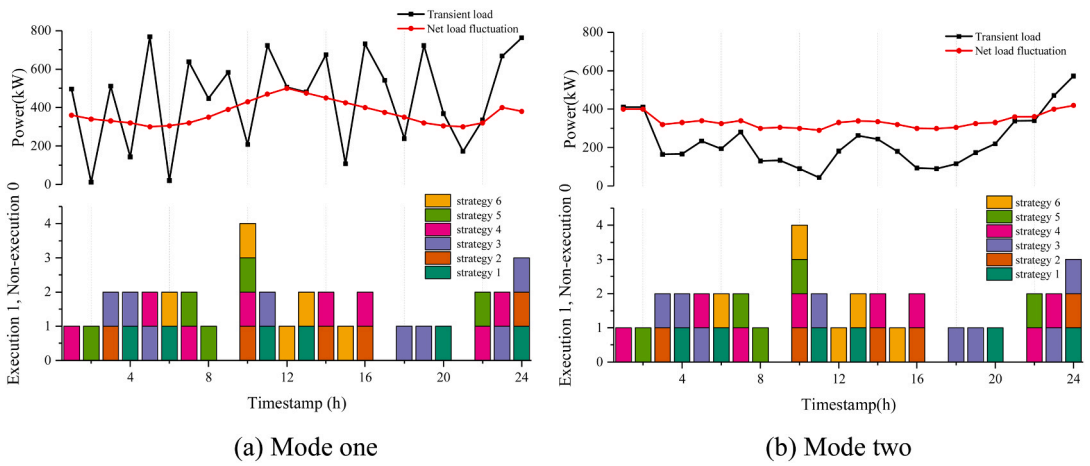

Fig. 12. Transient load and routing strategy (SDAFSA).

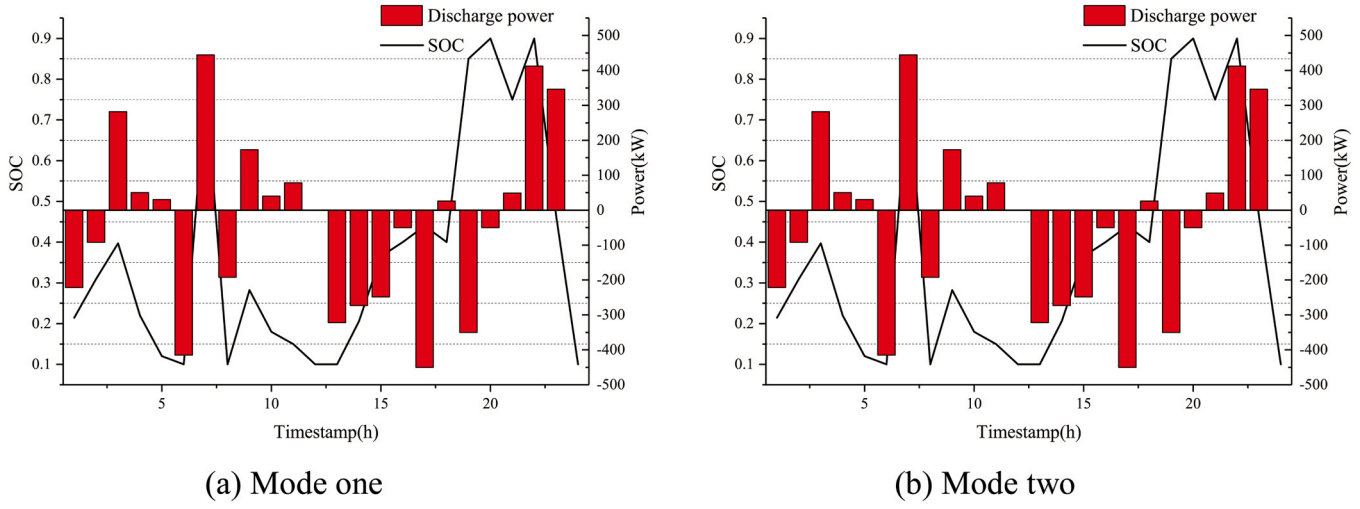

Fig. 13. Energy storage strategy (DEAFSA).

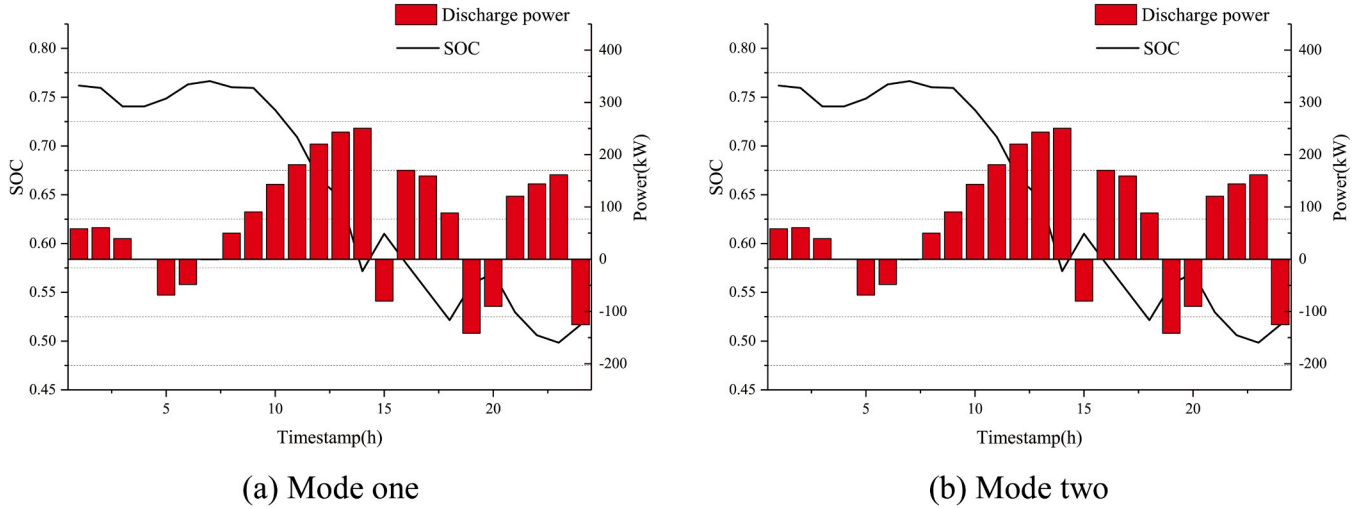

Fig. 14. Energy storage strategy (SDAFSA).

algorithm based on adaptive recombination behavior. This leads to higher accuracy in optimizing the transmission loss and hardware cost parameters of distributed units, while reducing computational costs, effectively reducing the overall economic cost of the system.

Comparative experiments on optimization methods show that the proposed method achieves a 7.97 % −9.98 % reduction in economic

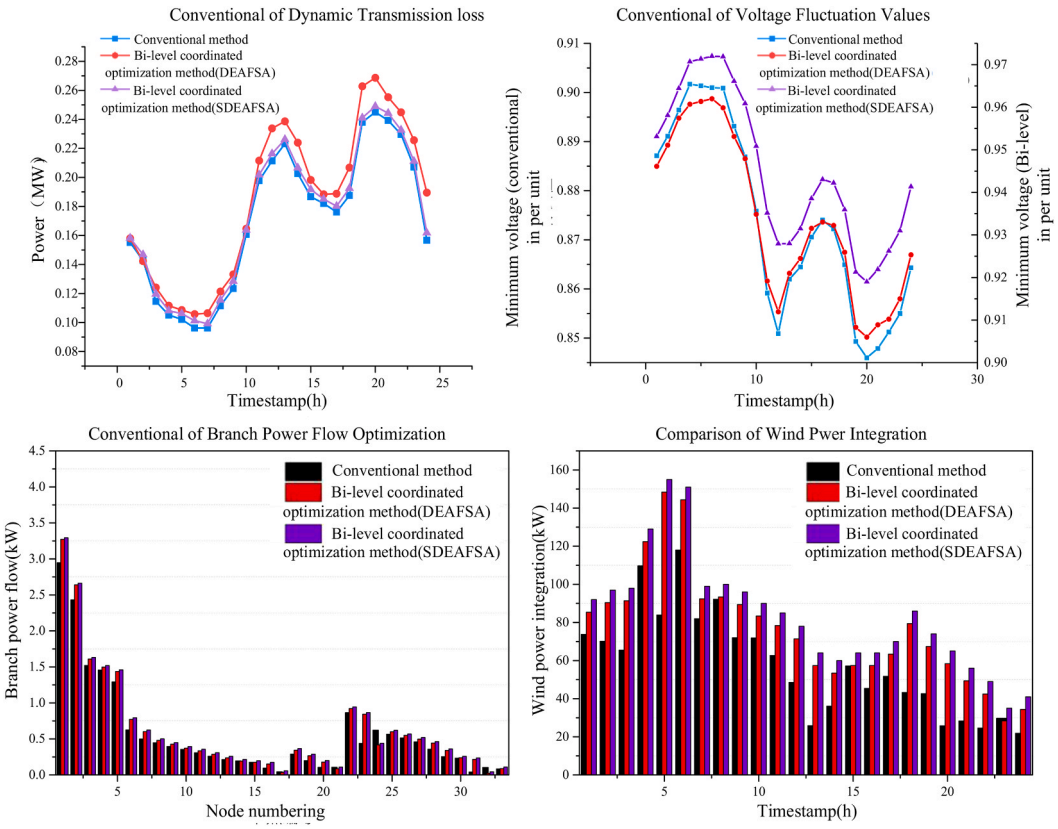

(a) Mode one

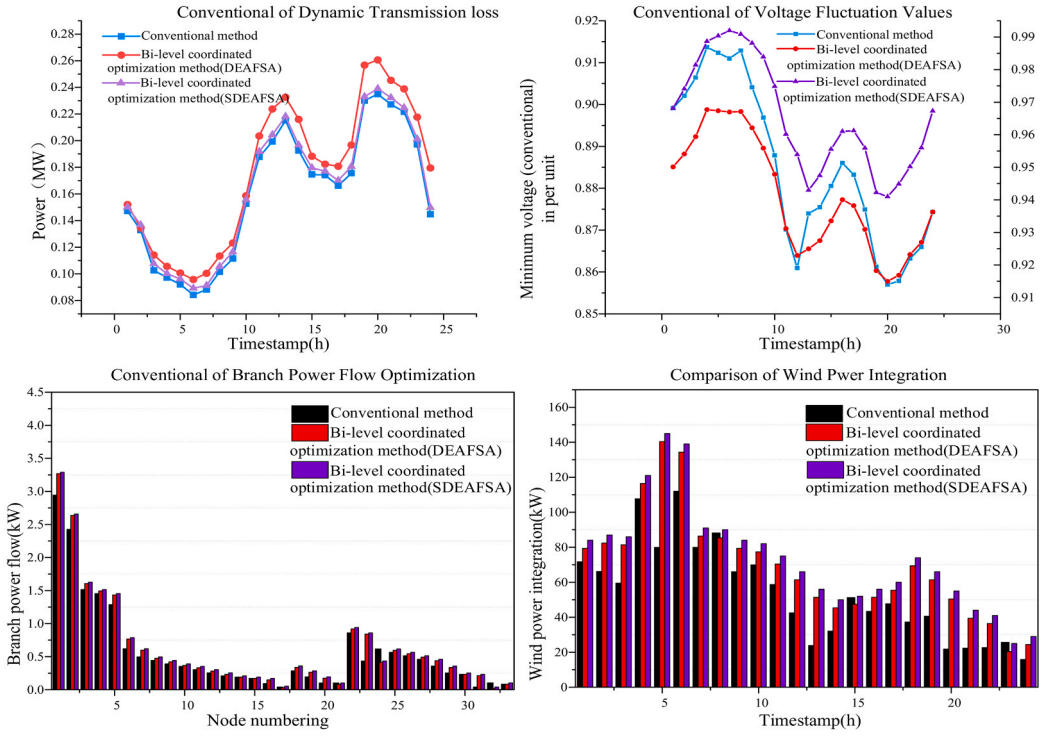

(b) Mode two

Fig. 15. Comparison before and after improvement (DEAFSA).

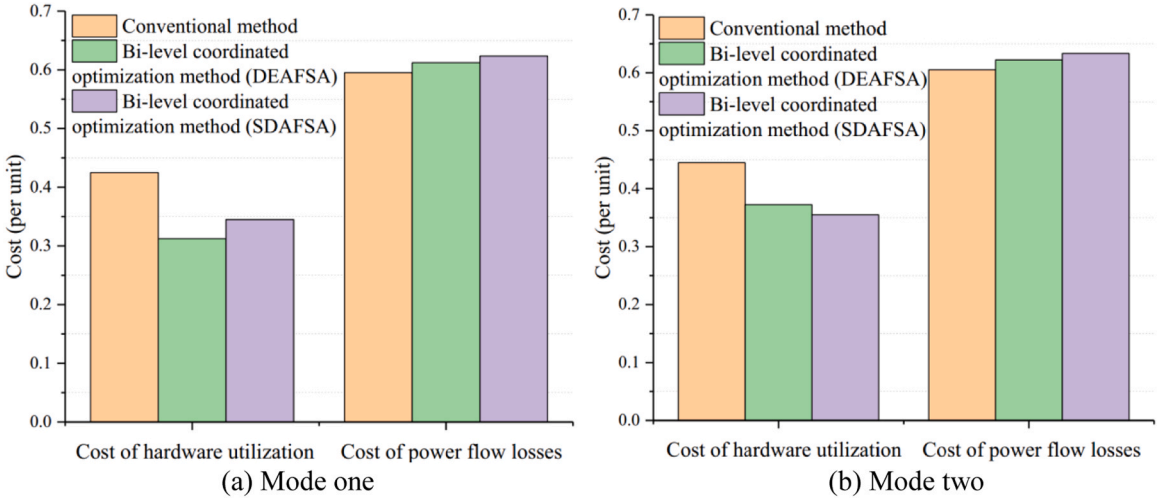

Fig. 16. Comparison chart of integrated economic costs.

costs by coordinating network losses and hardware costs, while maintaining a slight increase in network losses. Under the same total capacity of shore power, SDAFSA improves voltage stability by 1.11 % −2.22 % compared to DEAFSA, reduces branch flow losses by about 3.1 % −3.7 %, and increases wind power consumption by about 6.91 % −8.81 % before and after improvement. The introduction of the hardware cost model has indeed achieved the coordinated optimization of distributed unit network loss and hardware cost. Cost comparison calculations and algorithm performance experiments show that the adaptive recombination behavior adopted by this method improves optimization accuracy without significantly increasing resource consumption. As a result, the optimization performance of the double-layer coordinated optimization method in terms of transmission loss, power quality, and hardware usage cost has been further improved.

The method proposed in this paper has been validated on a medium-scale IEEE 33-node system. Future work will focus on extending the approach to larger-scale systems such as the IEEE 118-node network or practical urban distribution grids with multiple interconnected microgrids. Further efforts will also be dedicated to developing simplified models and distributed computing strategies, as well as introducing reinforcement learning-based parameter auto-tuning mechanisms. These enhancements are expected to strengthen the applicability of the method in smart grids and electric vehicle integrated energy systems, supporting more dynamic and high-dimensional operational scenarios.

CRediT authorship contribution statement

Yuxing Dai: Supervision, Formal analysis, Conceptualization. **Wen Hu:** Visualization, Supervision. **Kamal Al-Haddad:** Methodology, Formal analysis. **Zishun Peng:** Supervision, Software. **Cao Li:** Writing – review & editing, Validation, Software. **Yehong Li:** Writing – review & editing, Writing – original draft, Validation.

Declaration of Competing Interest

The authors declare that they have no known competing financial interests or personal relationships that could have appeared to influence the work reported in this paper.

Acknowledgements

This research was supported by Zhejiang Provincial Natural Science Foundation of China under Grant No. LTGS24E070002, the Dongguan Key Research & Development Program, China No. 20231200300142, and the Wenzhou Basic Scientific Research project funding No. H20220007.

Data availability

The data that has been used is confidential.

References

Abomazid, A.M., El-Taweel, N.A., Farag, H.E.Z., 2022. Optimal energy management of hydrogen energy facility using integrated battery energy storage and solar photovoltaic systems. IEEE Trans. Sustain. Energy 13, 1457–1468. https://doi.org/10.1109/TSTE.2022.3161891.

Al-Ismail, F.S., 2020. Discussion on “a new formulation of distribution network reconfiguration for reducing the voltage volatility induced by distributed generation, 4974–4974 IEEE Trans. Power Syst. 35. https://doi.org/10.1109/TPWRS.2020.3012366.

An, S., Wang, H., Leng, X., 2022. Optimal operation of multi-micro energy grids under distribution network in southwest china, 118461. Appl. Energy 309. https://doi.org/10.1016/j.apenergy.2021. . 118461.

Arnström, D., Bemporad, A., Axehill, D., 2022. A linear programming method based on proximal-point iterations with applications to multi-parametric programming. IEEE Control Syst. Lett. 6, 2066–2071. https://doi.org/10.1109/LCSYS.2021.3138218.

Azizi, A., Vahidi, B., Nematollahi, A.F., 2023. Reconfiguration of active distribution networks equipped with soft open points considering protection constraints. J. Mod. Power Syst. Clean. Energy 11, 212–222. https://doi.org/10.35833/MPCE.2022.000425.

Bayat, Mohammad, Aghabigloo, Masoud, Ghadimi, Ali Asghar, 2025. A generalized superposition-based method for loss allocation in active distribution networks: introducing effective current concept. ISSN 0142-0615 Int. J. Electr. Power Energy Syst. 169, 110740. https://doi.org/10.1016/j.ijepes.2025.110740.

Bazi, Y., Alajlan, N., Melgani, F., AlHichri, H., Malek, S., Yager, R.R., 2014. Differential evolution extreme learning machine for the classification of hyperspectral images. IEEE Geosci. Remote Sens. Lett. 11, 1066–1070. https://doi.org/10.1109/LGRS.2013.2286078.

Chen, L., Yaxin, L., Kai, W., Dongping, Z., Hu, L., 2023. Research on graph clustering based line loss prediction in low-voltage distribution network. 2023 2nd Asia Power Electr. Technol. Conf. (APET) Shanghai China 540–545. https://doi.org/10.1109/APET59977.2023.10489816.

Chen, T., Song, Y., Hill, D.J., Lam, A.Y.S., 2022. Chance-constrained opf in droop-controlled microgrids with power flow routers. IEEE Trans. Smart Grid 13, 2601–2613. https://doi.org/10.1109/TSG.2022.3154151.

Chennaif, M., Maaouane, M., Zahboune, H., Elhafyani, M., Zouggar, S., 2022. Tri-objective techno-economic sizing optimization of off-grid and ongrid renewable energy systems using electric system cascade extended analysis and system advisor model. Appl. Energy 305, 117844. https://doi.org/10.1016/j.apenergy.2021.117844.

Chew, B.S.H., Xu, Y., Wu, Q., 2019. Voltage balancing for bipolar dc distribution grids: A power flow based binary integer multi-objective optimiza-tion approach. IEEE Trans. Power Syst. 34, 28–39. https://doi.org/10.1109/TPWRS.2018.2866817.

Fan, F., Kockar, I., Xu, H., Li, J., 2022. Scheduling framework using dynamic optimal power flow for battery energy storage systems. CSEE J. Power Energy Syst. 8, 271–280. https://doi.org/10.17775/CSEEJPES.2020.03710.

Gao, H., Ma, W., He, S., Wang, L., Liu, J., 2022. Time-segmented multi-level reconfiguration in distribution network: A novel cloud-edge collaboration framework. IEEE Trans. Smart Grid 13, 3319–3322. https://doi.org/10.1109/TSG.2022.3156433.

Gao, S., Jia, H., Marnay, C., 2019. Techno-economic evaluation of mixed ac and dc power distribution network for integrating large-scale photovoltaic power generation. IEEE Access 7, 105019–105029. https://doi.org/10.1109/ACCESS.2019.2931985.

Huang, L., Liao, L., Wu, C.H., 2015. Evolutionary model selection and parameter estimation for protein-protein interaction network based on differential evolution algorithm. IEEE/ACM Trans. Comput. Biol. Bioinforma. 12, 622–631. https://doi.org/10.1109/TCBB.2014.2366748.

Huang, L., Lai, C.S., Zhao, Z., Yang, G., Zhong, B., Lai, L.L., 2023. Robust n − k security-constrained optimal power flow incorporating preventive and corrective generation dispatch to improve power system reliability. CSEE J. Power Energy Syst. 9, 351–364. https://doi.org/10.17775/CSEEJPES.2021.06560.

Huang, W., Zheng, W., Hill, D.J., 2021. Distribution network reconfiguration for short-term voltage stability enhancement: an efficient deep learning approach. IEEE Trans. Smart Grid 12, 5385–5395. https://doi.org/10.1109/TSG.2021.3097330.

Lejeune, M.A., Dehghanian, P., 2020. Optimal power flow models with probabilistic guarantees: a boolean approach. IEEE Trans. Power Syst. 35, 4932–4935. https://doi.org/10.1109/TPWRS.2020.3016178.

Li, T., Yang, F., Zhang, D., Zhai, L., 2021. Computation scheduling of multiaccess edge networks based on the artificial fish swarm algorithm. IEEE Access 9, 74674–74683. https://doi.org/10.1109/ACCESS.2021.3078539.

Li, Ye, Hu, Zhijian, Li, Tiange, Sha, Licheng, Zhang, Zaichi, 2025. Flexible scheduling strategy considering multifaceted flexible resources and transmission-distribution network cooperative optimization. ISSN 2352-4847 Energy Rep. 13, 2892–2906. https://doi.org/10.1016/j.egyr.2025.02.028.

Liu, B., Peng, Y., Xu, J., Mao, C., Wang, D., Duan, Q., 2021. Design and implementation of multiport energy routers toward future energy internet. IEEE Trans. Ind. Appl. 57, 1945–1957. https://doi.org/10.1109/TIA.2021.3057345.

Liu, Y., Li, J., Wu, L., 2019. Coordinated optimal network reconfiguration and voltage regulator/der control for unbalanced distribution systems. IEEE Trans. Smart Grid 10, 2912–2922. https://doi.org/10.1109/TSG.2018.2815010.

Macedo, L.H., Franco, J.F., Rider, M.J., Romero, R., 2015. Optimal operation of distribution networks considering energy storage devices. IEEE Trans. Smart Grid 6, 2825–2836. https://doi.org/10.1109/TSG.2015.2419134.

Mahdavi, M., et al., 2024b. A mixed-integer programming model for reconfiguration of active distribution systems considering voltage dependency and type of loads and renewable sources. IEEE Trans. Ind. Appl. 60 (4), 5291–5303. https://doi.org/10.1109/TIA.2024.3383805.

Mahdavi, M., Awaafo, A., Schmitt, K., Chamana, M., Jurado, F., Bayne, S., 2024a. An effective formulation for minimizing distribution network costs through distributed generation allocation in systems with variable loads. IEEE Trans. Ind. Appl. 60 (4), 5671–5680. https://doi.org/10.1109/TIA.2024.3382255.

Mahdavi, Meisam, Soleimani, Alireza, Pinnarelli, Anna, Heidari, Mehran, Jurado, Francisco, 2025. Cost-based optimization of DG and capacitor placement in distribution networks under dynamic load conditions. ISSN 2352-4847 Energy Rep. 13, 5525–5534. https://doi.org/10.1016/j.egyr.2025.05.017.

Miao, J., Zhang, N., Kang, C., Wang, J., Wang, Y., Xia, Q., 2018. Steady-state power flow model of energy router embedded ac network and its application in optimizing power system operation. IEEE Trans. Smart Grid 9, 4828–4837. https://doi.org/10.1109/TSG.2017.2672821.

Mirjalili, S., Mirjalili, S.M., Lewis, A., 2014. Grey wolf optimizer. Adv. Eng. Softw. 69, 46–61. https://doi.org/10.1016/j.advengsoft.2013.12.007.

Rahman, M.A., Islam, M.R., Muttaqi, K.M., Sutanto, D., 2020. Data-driven coordinated control of converters in a smart solid-state transformer for reliable and automated distribution grids. IEEE Trans. Indust ry Appl. 56, 4532–4542. https://doi.org/10.1109/TIA.2020.2972507.

Song, Y., Hill, D.J., Liu, T., Chen, T., 2022. Convex relaxation of ac optimal power flow with flexible transmission line impedances. IEEE Trans. Power Syst. 37, 3129–3132. https://doi.org/10.1109/TPWRS.2022.3164590.

Sotiroudis, S.P., Goudos, S.K., Gotsis, K.A., Siakavara, K., Sahalos, J.N., 2013. Application of a composite differential evolution algorithm in optimal neural network design for propagation path-loss prediction in mobile communication systems. IEEE Antennas Wirel. Propag. Lett. 12, 364–367. https://doi.org/10.1109/LAWP.2013.2251994.

Sun, T., Sun, X.-M., 2021. An adaptive dynamic programming scheme for nonlinear optimal control with unknown dynamics and its application to turbofan engines. IEEE Trans. Ind. Inform. 17, 367–376. https://doi.org/10.1109/TII.2020.2979779.

Tavalaei, Hadi, Samiei Moghaddam, Mahmoud, Vahedi, Mojtaba, Salehi, Nasrin, Hoseini Abardeh, Mohamad, 2024. Energy management in smart distribution networks: Synergizing network reconfiguration, energy storage, and electric vehicles with disjunctive convex hull relaxation. ISSN 2352-4847 Energy Rep. 12, 5999–6015. https://doi.org/10.1016/j.egyr.2024.11.085.

Wang, R., Jiang, S., Ma, D., Sun, Q., Zhang, H., Wang, P., 2022. The energy management of multiport energy router in smart home. IEEE Trans. Consum. Electron. 68, 344–353. https://doi.org/10.1109/TCE.2022.3200931.

Wu, T., Zhao, C., Zhang, Y.-J.A., 2021. Distributed ac-dc optimal power dispatch of vsc-based energy routers in smart microgrids. IEEE Trans. Power Syst. 36, 4457–4470. https://doi.org/10.1109/TPWRS.2021.3056768.

Xiao, X., Li, Z., Wang, Y., Zhou, Y., Liu, K., 2022. Optimal power quality compensation of energy storage system in distribution networks based on unified multi-phase opf model. IEEE Trans. Smart Grid 13, 1873–1887. https://doi.org/10.1109/TSG.2022.3146464.

Yang, T., Guo, Y., Deng, L., Sun, H., Wu, W., 2021. A linear branch flow model for radial distribution networks and its application to reactive power optimization and network reconfiguration. IEEE Trans. Smart Grid 12, 2027–2036. https://doi.org/10.1109/TSG.2020.3039984.

Zhao, X., Liu, Y., Chai, X., Guo, X., Wang, X., Zhang, C., Wei, T., Shi, C., Jia, D., 2022. Multimode operation mechanism analysis and power flow flexible control of a new type of electric energy router for low-voltage distribution network. IEEE Trans. Smart Grid 13, 3594–3606. https://doi.org/10.1109/TSG.2022.3170936.

Zheng, W., Wu, W., Zhang, B., Sun, H., Liu, Y., 2016. A fully distributed reactive power optimization and control method for active distribution networks. IEEE Trans. Smart Grid 7, 1021–1033. https://doi.org/10.1109/TSG.2015.2396493.

Zheng, W., Huang, W., Hill, D.J., Hou, Y., 2021. An adaptive distributionally robust model for three-phase distribution network reconfiguration, IEEE s. Trans. Smart Grid 12, 1224–1237. https://doi.org/10.1109/TSG.2020.3030299.

Zhu, Y., Gao, H., 2020. Improved binary artificial fish swarm algorithm and fast constraint processing for large scale unit commitment. IEEE Access 8, 152081–152092. https://doi.org/10.1109/ACCESS.2020.3015585.